Chapter 11

Evanescent Wave Biosensors with a Hydrogel Binding Matrix

Jakub Dostalek,* Yi Wang, Chun Jen Huang, and Wolfgang Knoll
AIT Austrian Institute of Technology, Vienna, 1220, Austria
*jakub.dostalek@ait.ac.at

Hydrogels have become widely used materials in numerous important fields such as drug delivery and tissue engineering and have allowed great improvements in the performance of analytical and bioanalytical technologies for detection of chemical and biological species. Their highly open structure makes them attractive to serve as a binding matrix that can accommodate large amounts of target analyte, provide a natural microenvironment for biomolecular recognition elements, and enable design of surfaces that can resist nonspecific adsorption from complex samples for highly specific biosensor devices. In addition, a special class of "smart" hydrogels responsive to external stimuli (e.g., through temperature or pH changes) holds potential for development of biosensors with enhanced sensitivity and implementing of new biosensor schemes for sensitive analysis of molecular analytes. This chapter provides an overview of recent advances in our and other laboratories, as well as practical leads for design, characterization, and implementation of hydrogel surface architectures for ultrasensitive affinity biosensors based on evanescent wave optics.

11.1 Introduction

Hydrogels are insoluble, cross-linked, water-swollen polymer networks of hydrophilic homopolymers or copolymers. Owing to their highly open structure and large inner surface, hydrogels can accommodate large amounts of molecules with specific functions. Hydrogels become irreplaceable materials in numerous important areas ranging from pharmaceutical applications (e.g., drug delivery and tissue engineering) [1-6] to biosensor technologies for detection of chemical or biological analytes [7-12]. In biosensor applications, hydrogel materials are

Book Title
First Author & Second Author

www.panstanford.com

employed at an interface between an analyzed sample and a transducer. Typically, hydrogels are modified with biomolecular recognition elements (BREs) such as antibodies, enzymes, or biomimetic moieties based on molecular imprinting in order to specifically recognize target analytes present in a liquid sample (Figure 11.1). Compared with other types of biointerfaces (e.g., based on self-assembled monolayers [SAMs]), hydrogels can accommodate orders-of-magnitude larger amounts of recognition elements and provide a more natural microenvironment for biomolecules, which increases their stability and offer routes for implementing additional functionalities (e.g., separation of target analyte from other molecules in a sample, simplified methods for readout). In addition, the class of "smart" gels that can respond to external stimuli become of interest for development of entirely new biosensor schemes. For instance, miniature hydrogel sensor elements were integrated in a contact lens for the analysis of glucose in tear fluid. The hydrogel element served both as a host for recognition elements and as an optical transducer for detection of glucose [13].

In this chapter, we focus on biosensors in which hydrogel-based binding matrices with thicknesses up to micrometers are probed by an evanescent field of surface plasmon (SP) and optical waveguide waves. The optical detection of analyte-binding events is carried out through monitoring of binding-induced refractive index changes or by fluorescence spectroscopy. We discuss key performance characteristics of hydrogel-based binding matrices and their implementation in biosensor devices. Let us note that detailed information on the synthesis and characterization of hydrogels and their application in other areas can be found in chapter 10. Thinner polymer brushes developed for biosensor applications are discussed in chapter 5.

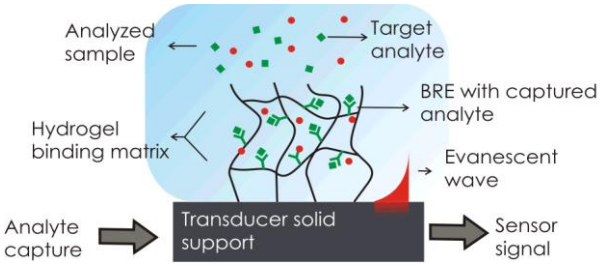

Figure 11.1 (a) Scheme of a hydrogel-based biointerface on top of a biosensor surface for detection of molecular analytes.

11.2 Key Characteristics of Hydrogel Binding Matrices

Various polymers were synthesized for hydrogel biointerface architectures as reported in the literature. These include alginate [14], dextran [15], poly(vinylalcohol) (PVA) [16], 2-hydroxyethyl methacrylate (HEMA) [17, 18], poly(2-vinylpyridine) (P2VP) [19, 20], polyethylene glycol (PEG) acrylate [21],

and poly(N-isopropylacrylamide) (PNIPAAm) [22, 23]. In addition, sol-gels that are formed by the polymerization of silicate monomers were applied for development of microporous matrices in which analyte-sensitive species can be entrapped with large densities and small analyte molecules diffuse [24]. Compared with inorganic porous films explored for the construction of binding matrices (e.g., porous silicon [25, 26], aluminum oxides [27, 28], silicon dioxide [29], titanium oxide [30]), soft hydrogel-based matrices provide a platform offering the advantage of better biocompatibility, flexible functionalization, and tunable characteristics that can be often controlled through external stimuli. In the following section, we discuss characteristics of hydrogels that are essential for development of hydrogel-based binding matrices.

11.2.1 Swelling properties

For fast biosensor detection times, target analytes have to rapidly diffuse through the hydrogel binding matrix and react with incorporated recognition elements. The mesh size ξ and the molecule hydrodynamic radius r_h are the key parameters affecting the diffusion-driven mass transport in gels in which the diffusion coefficient scales as $D_g \sim \exp(-r_h/\xi)$. In highly swollen gels with $r_h << \xi$, D_g of mobile target molecules is close to that in water and recognition elements in hydrogels are easily accessible for the binding. However, diffusion is dramatically hindered by steric and hydrodynamic interactions when the size of the mobile molecules is comparable to the mesh size $r_h \sim \xi$. The distance between polymer cross-links provides a measure for the mesh size ξ, and it is related to the hydrogel swelling ratio Q, defined as the ratio of the hydrogel film thickness in swollen (hydrated) and collapsed (dry) states. The swelling ratio Q is inversely proportional to the polymer volume fraction f. These parameters can be controlled through the gel composition and cross-linking density, as described in chapter 10 in more detail.

PNIPAAm and dextran-based hydrogel binding matrices with the polymer volume fraction $f \sim 0.1$ were successfully applied in evanescent wave biosensors for detection of protein molecules [15, 23]. For a functionalized PNIPAAm-based hydrogel with $f \sim 0.1$, Huang *et al.* estimated that the diffusion coefficient of immunoglobulin G (IgG) (hydrodynamic radius $r_h = 6$ nm [31]) was close to 10^{-6} $mm^2\,s^{-1}$ [32], which is more than an order of magnitude lower than in water ($D = 3\times10^{-5}$ mm^2s^{-1}). Raccis *et al.* measured a diffusion coefficient of $D_g \sim 10^{-5}$ mm^2s^{-1} for green fluorescence protein (GFP, hydrodynamic radius $r_h = 2.3$ nm [33]) in a similar PNIPAAM gel with the polymer volume content $f \sim 0.05$ by fluorescence correlation spectroscopy (FCS) [34]. A special class of "smart" responsive hydrogels can change swelling characteristics through an applied external stimulus such as temperature or pH. Hydrogels can be sensitized to other types of stimuli including light irradiation (through incorporation of metallic nanoparticles supporting localized SP [35]) and a magnetic field (through their

modification by magnetic nanoparticles [36, 37]). The characteristic time of the hydrogel film response to the stimuli scales with its thickness d_h and diffusion coefficient D of the network as $\sim d_h^2/D$, where D is in the order of 10^{-4}–10^{-6} mm^2s^{-1} for most common gels [9].

11.2.2 Antifouling properties

The development of polymer films that are resistant against fouling by molecular, cellular, and other species present in complex samples (e.g., blood and sea water) is a major challenge in the field of biomaterials research. In biosensor applications, the capability of a biointerface to selectively capture target molecules from a sample strongly depends on its antifouling properties. Although general physical and chemical properties that make surface antifouling are still under research, the following conditions were identified to be necessary for good resistance against nonspecific sorption: (i) zero net charge, (ii) hydrophilic nature, and presence of groups that are (iii) hydrogen bond acceptors but (iv) not hydrogen bound donors [38-40]. Furthermore, the permeability of the hydrogel layer may also affect the antifouling properties of the surface, since the low porosity of the hydrogel may hinder interactions with large biomolecules. Traditionally, PEG-based polymers are employed for surfaces that exhibit good resistance against nonspecific sorption. Recently, improved antifouling properties were reported for polymer surfaces with nanometer-scale homogenous mixtures of either zwitterionic or charged groups [41].

For instance, the Jiang group has demonstrated that ultra-low nonspecific adsorption (< 3 pg/mm^2) of blood plasma occurred on the top of compact films composed of poly(sulfobetaine) and poly(carboxybetaine) polymers with the thickness of several tens of nanometers [42, 43]. The same group studied other dense polymers that contained mixed moieties of aminoethyl methacrylate hydrochloride and carboxyethyl acrylate. They showed that these surfaces with tuned charge characteristics can minimize the adsorption of fibrinogen [43]. The Tabrizian group has developed a composite cross-linked hydrogel with the thickness of a few nanometers consisting of carboxymethyl cellulose (CMC), polyethyleneimine (PEI), and PEG. They showed that on a thin CMC-PEG-PEI hydrogel film, nonspecific sorption of 1.1 ng/mm^2 occurred from 25% serum [44]. Masson *et al.* have investigated antifouling properties of three-dimensional (3D) open structures that were composed of carboxymethylated (CM) dextran [45]. Their results indicated that the nonspecific binding from bovine serum was increasing from 2.3 to 230 ng/mm^2 (depending on the molecular weight of CM dextran chains between 2 and 5,000 kDa). In addition, they showed several-fold improvement of the nonspecific interactions by using other biocompatible polymer derivatives, including CM hyaluronic acid. Wang *et al.* showed that nonspecific sorption from blood serum into an open structure of cross-linked dextran hydrogel with a thickness of around 1 μm can be lowered by premixing an analyzed sample with dextran chains to a value as low as 2 ng/mm^2. [15]. Aulasevich *et al.* investigated antifouling properties of a highly swollen PNIPAAm-based film with a thickness of around 2 μm and polymer volume

content of f ~ 0.1. They reported a mass of adsorbed proteins from undiluted human serum of 5 ng/ mm^2 [46]. These values are significantly higher compared with previous examples due to the larger surface area of the 3D gel.

11.2.2 Modification of hydrogel with catcher molecules

In order to specifically capture the target analyte from a sample, recognition moieties have to be incorporated in a hydrogel film attached to the biosensor surface. Most often, hydrogel-based biointerfaces are modified with biomolecular recognition elements such as antibodies, complementary DNA, or enzymes by using covalent or affinity-based coupling to flexible polymer chains. More recently, alternative biomimetic approaches based on molecular imprinting are pursued for biosensor applications [47, 48].

Compared with highly cross-linked, molecular imprinted polymer (MIP) structures, the imprinting of hydrogels offers the advantage of increased binding capacity and responsive properties. Recent works indicated that this type of weakly cross-linked polymers is promising for imprinting of larger molecules such as proteins [49] or even cells [50]. With respect to more traditional biomolecular recognition elements (e.g., antibodies), MIP-based materials hold potential to provide more robust and cost-effective means for specific capture of target analytes. For several small molecules, MIP structures with affinity binding constants comparable to those obtained for immunoassays were reported [51]. In general, MIPs are formed by co-polymerization of functional monomers in the presence of the target analyte (template) that is subsequently removed by washing and/ or extraction (see Figure11. 1). The imprinted polymer carries specific cavities that are complementary in size and shape to the target analyte. The binding cavities for the target molecules are formed via reversible covalent bonds or via noncovalent interactions such as hydrogen bonds, electrostatic interaction, hydrophobic interactions, or van der Waals forces between polymer monomers and target molecule on [52, 53].

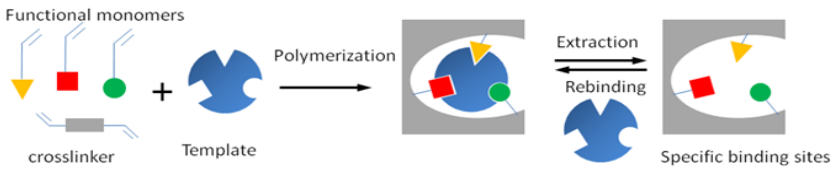

Figure11. 1 Schematic representation of the molecular imprinting principle.

Chemical attachment of biomolecular recognition elements is mostly carried out by using carboxylic or amino groups in a gel [46, 54-58]. The carboxylic acid group can be activated by reaction with chemicals such as 1-ethyl-3-(3-dimethylaminopropyl)-carbodiimide) (EDC) and N-hydroxysulfosuccin-imide (sulfo-NHS) to form the sulfo-NHS ester (see Figure 11.2a). The Sulfo-NHS

ester can react with the amino groups to form a stable linkage between a gel and a biomolecule. Another active ester coupling has been developed based on the activation of carboxylic moieties by using a mixture of EDC and sodium *para*-tetrafluorophenol sulfonate (TFPS), as shown in Figure 11.2b. As TFPS is negatively charged, biomolecules can be efficiently loaded into the activated gel from a buffer with pH that is lower than the biomolecule isoelectric point through Columbic interaction [46]. Moreover, a range of other coupling strategies can be used based on converting carboxylic groups to other chemical moieties such as biotin, thiol, and aldehyde (see Figure 11.2c).

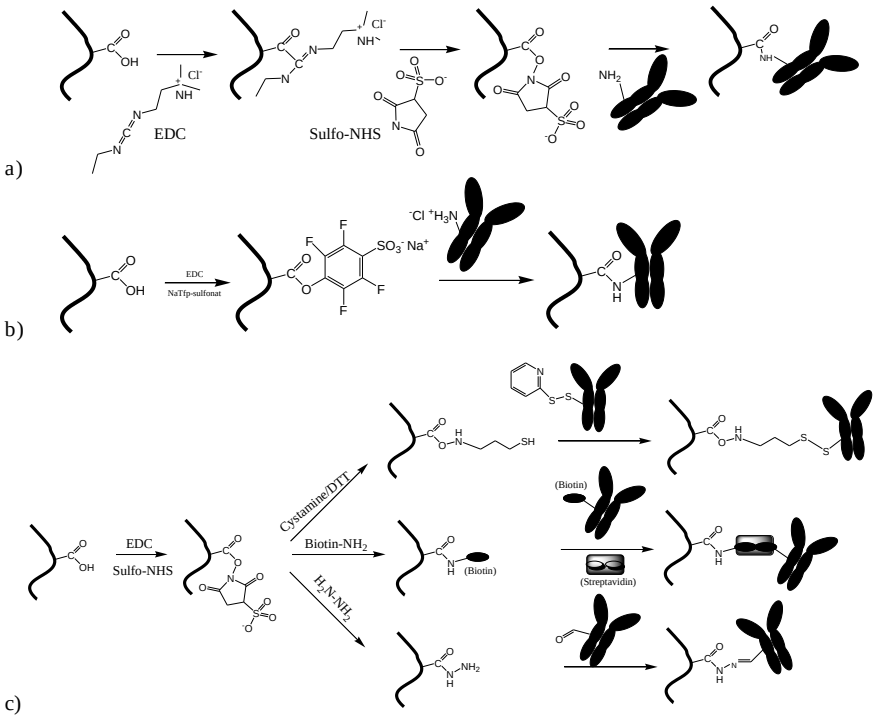

Figure 11.2 Schematic of amine coupling of biomolecules by (a) EDC/ NHS and (b) EDC/ TFPS esters. (c) Conjugation of biomolecules via thiol, biotin, and aldehyde moieties.

11.3 Evanescent Wave Optics for Probing Hydrogel Films

Upon total internal reflection (TIR) of light at a boundary between dielectrics with different refractive indices, an evanescent electromagnetic field that exponentially decays into the lower refractive index medium can be generated. As seen in Figure 11.3, the evanescent wave probes the lower refractive index medium with the penetration depth:

$$L_p = \frac{1}{\sqrt{\beta^2 - k_0^2 n_d^2}}, \tag{11.1}$$

where $k_0 = 2\pi/\lambda$ is the propagation constant of light with the wavelength λ in vacuum, $\beta = k_0 n_p \sin(\theta)$ is the component of light propagation constant in the high refractive index dielectric that is parallel to the interface, and n_d and n_p are the refractive indices of the lower and the higher refractive index dielectric, respectively. The angle of incidence of the light beam in the higher refractive index dielectric θ is higher than the critical angle $\theta_c = \sin^{-1}(n_{d/} n_p)$.

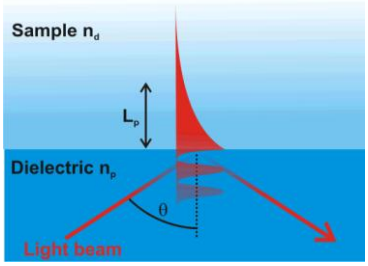

Figure 11.3 TIR of a light beam at an interface between dielectrics with refractive indices of n_p and n_d.

Guided waves supported by a layer structure on a sensor surface represent evanescent waves that are excellently suited for an observation of hydrogel films and molecular interactions. Changes in gels that are associated with refractive index variations can be measured through spectroscopy of guided waves [46] and advanced schemes of fluorescence-based detection allow measurement of molecular binding events [15]. Further, we discuss SP and dielectric waveguide waves for probing of thin hydrogel films.

11.3.1 Surface plasmon waves

SPs are guided waves propagating along a metal dielectric interface that originate from coupled oscillations of electron plasma and the associated electromagnetic field. The SP propagation constant β is equal to:

$$\beta = \frac{2\pi}{\lambda}\sqrt{\frac{n_m^2 n_d^2}{n_m^2 + n_d^2}}, \tag{11.2}$$

where n_d is the refractive index of a dielectric and n_m is the refractive index of metal. As Figure 11.4a shows, the profile of the electromagnetic field of SP is evanescent into both metal and dielectric media. The SP penetration depth L_p into a metal is typically below 10 nm and its field is mostly propagating in a dielectric. For instance, at a boundary between gold and water with $n_d = 1.33$, the penetration depth into a dielectric reach $L_p = 180$ nm for the wavelength $\lambda = 633$ nm.

Another type of SP waves can be observed on a thin metal film sandwiched by dielectrics with similar refractive indices of $n_d \sim n_b$ (see Fig. 11.5b). For thickness of the metal film lower than ~ 50 nm, SPs propagating on opposite interfaces become strongly coupled and two new modes are established [59]. These modes

are referred to as long-range surface plasmon (LRSP with anti-symmetrical electric field component parallel the surface) and short-range surface plasmon (SRSP with symmetrical electric field component parallel the surface). LRSP waves are weaker guided by the metal and thus exhibit a more extended field profile and lower losses than regular SP on an individual metal interface. By optimizing the metal thickness and through introducing a small perturbation to the symmetry (e.g., n_b is slightly lower than n_d), the penetration depth L_p of LRSPs can be tuned to reach up to several micrometers [60, 61].

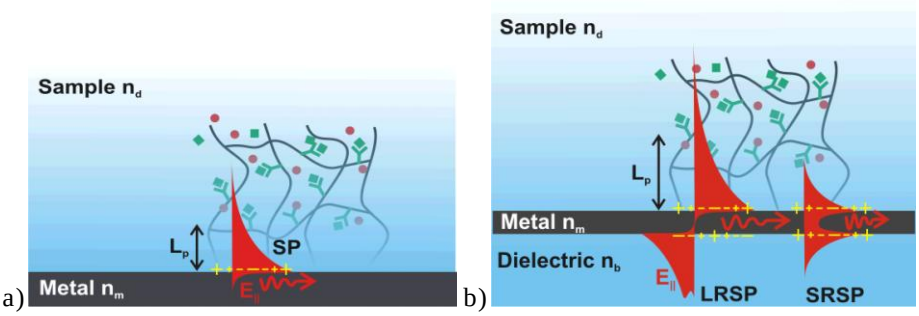

Figure 11.4 (a) SP propagating along a metal surface. (b) LRSP and SRSP, respectively, supported by a thin metallic film embedded in media with similar refractive indices of n_d and n_b.

A layer structure with two metallic films was developed for simultaneous probing of a sensor surface with an extended field of two LRSPs modes exhibiting different profiles [62]. These modes originate from coupling of LRSPs across the gap between two metallic films, as shown at the bottom of Figure 11.5. For the structure with a fluoropolymer buffer layer between the metallic films with a thickness of 640 nm and metallic films with a thickness of d_m = 22.5 nm, the sensor surface in contact with water can be probed by strong LRSP fields with different penetration depths of L_p = 364 and 950 nm (see Figure 11.5).

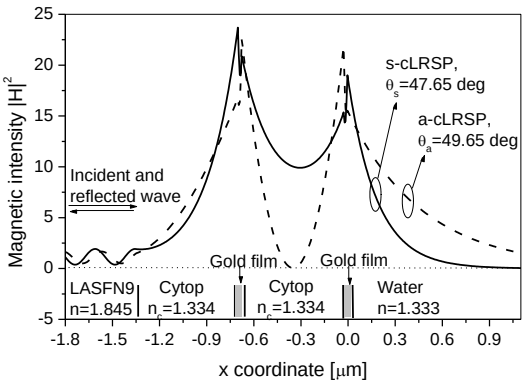

Figure 11.5 Profile of the magnetic field intensity of coupled LRSPs (noted as a-cLRSP and s-cLRSP) supported by a layer structure with two metallic films. (Reproduced with permission from [63]).

11.3.2 Hydrogel waveguide optical modes

A hydrogel film that is attached to a metallic surface can support guided light waves if its refractive index and the thickness are sufficiently large (see Fig. 11.6). These waves are confined in a gel through the reflecting metal at the inner interface and by TIR at the outer interface. The propagation constant β of hydrogel-guided waves can be determined by solving the following dispersion relation:

$$\tan\left(\kappa d_h\right) = \frac{\gamma_d n_h^2 / \kappa n_d^2 + \gamma_m n_h^2 / \kappa n_m^2}{1 - \left(\gamma_d n_h^2 / \kappa n_d^2\right)\left(\gamma_m n_h^2 / \kappa n_m^2\right)}, \tag{11.3}$$

where n_d is the refractive index of the liquid sample on the top of the gel, and n_h and d_h are refractive index and thickness of the hydrogel film, respectively. The terms $\kappa^2 = k_0^2 n_h^2 - \beta^2$, $\gamma_m^2 = \beta^2 - k_0^2 n_m^2$ and $\gamma_d^2 = \beta^2 - k_0^2 n_d^2$ are the transverse propagation constants in the hydrogel film, the metal, and the liquid, respectively.

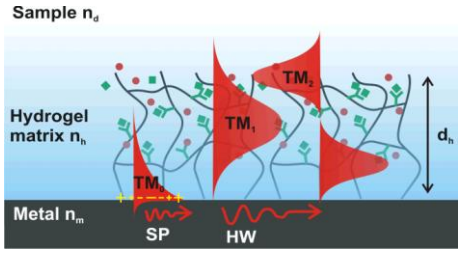

Figure 11.6 Hydrogel film attached to a metallic surface that serves as an optical waveguide.

11.3.3 Optical excitation of surface plasmon and hydrogel guided waves

In order to probe hydrogel films with SP and hydrogel waveguide (HW) waves, the attenuated total reflection (ATR) method with Kretschmann configuration can be used. The ATR method is a popular means for the excitation of guided waves, in which a light beam is launched to a prism with a high refractive index n_p and is reflected from its base under an angle of incidence θ that is higher than the critical angle $\theta > \theta_c$. On the prism base, a layer architecture supporting, for example, SP or HW waves is attached. The coupling between the light beam in the prism and the guided wave at the prism base occurs via their evanescent field in vicinity to (resonant) angles of incidence θ that fulfill the following phase-matching condition:

$$k_0 \sin\left(\theta\right) = \mathrm{Re}\{\beta\}. \tag{11.4}$$

Figure 11.7 shows a typical implementation of an ATR optical setup that is based on the so-called spectrometery of guided waves with angular modulation. The sensor chip is illustrated by a layer structure supporting LRSP and HW waves

deposited on a glass slide that is optically matched to the prism base. At the sensor surface, a flow-cell is attached in order to bring analyzed samples in contact with a hydrogel film. The assembly of the prism, sensor chip, and flow-cell is mounted on a rotation stage enabling the control of the angle of incidence θ of a laser beam propagating in the prism.

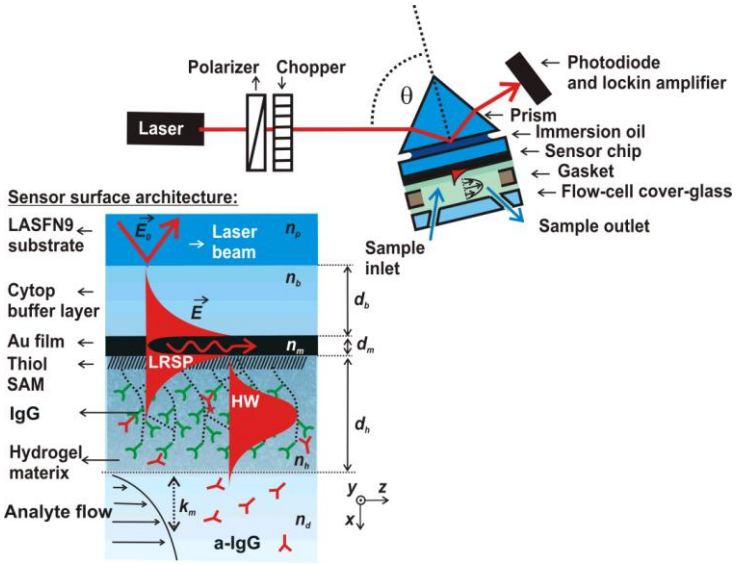

Figure 11.7 The ATR method with Kretschmann configuration for the excitation of LRSP and HW waves.

The interaction between a monochromatic light beam and guided waves on the sensor surface is manifested as a series of resonant dips in the angular reflectivity spectrum $R(\theta)$ located at angles for which the condition holds (see Figure 11.8a). Upon resonant coupling to SP and HW waves, the field intensity is enhanced through these waves propagating along the sensor surface. Figure 11.8b shows the characteristic profile of LRSP and HW modes excited in a layer structure consisting of a Cytop layer (refractive index $n_b = 1.337$ and thickness $d_b = 715$ nm), a gold film (thickness $d_m = 13.2$ nm), a hydrogel film (thickness $d_h = 1{,}800$ nm and refractive index $n_h = 1.345$), and an aqueous sample (refractive index $n_d = 1.333$). It shows that the LRSP field exponentially decays through the hydrogel film with a penetration depth of $L_p = 920$ nm. The field intensity of HW wave is confined in the hydrogel film, reaches its maximum in vicinity to its outer interface, and evanescently decays into the aqueous sample.

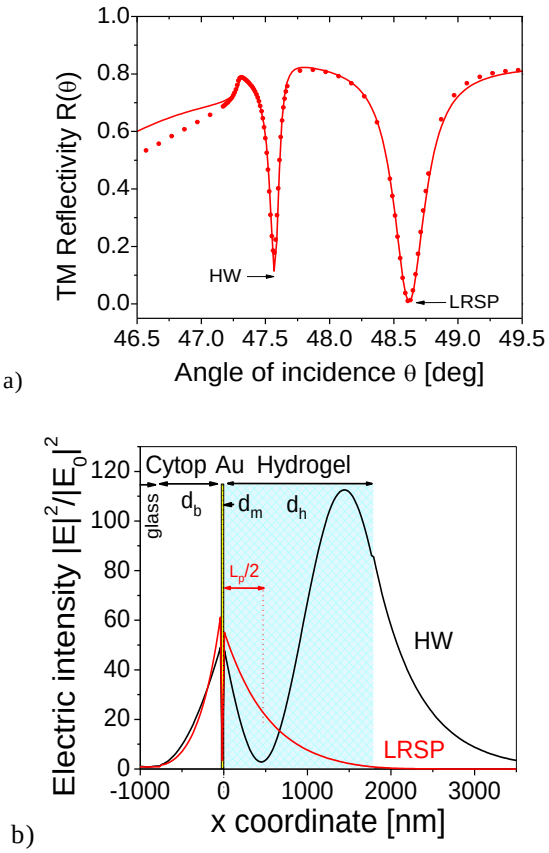

Figure 11.8 (a) Reflectivity spectrum and (b) field profile for the resonant coupling to LRSP and HW. (Reproduced with permission from [32]).

11.3.4 Observation of hydrogel films by spectroscopy of guided waves

Spectroscopy of SP and HW waves provides a powerful technique for *in situ* observation of hydrogel films. It allows real-time monitoring of changes in their characteristics such as thickness and density. For instance, Harmon *et al.* [64] have investigated volume-phase transitions in pNIPAAm hydrogel films as an effect of pressure and temperature by using SP resonance (SPR), Beines *et al.* studied swelling characteristics of thin responsive pNIPAAm by the spectroscopy of HW waves [22], and Aulasevich *et al.* employed spectroscopy of HW waves for the observation of molecular interactions in pNIPAAm hydrogel that was modified with protein molecules [46].

The reflectivity spectrum measured upon the coupling to guided waves propagating in a hydrogel film carries information on its refractive index profile. This profile can be determined through an analysis of the reflectivity spectrum by using an appropriate model (e.g., fitting with Fresnel equations for planar

films, as shown in Figure 11.9a). Compared with regular SPR that cannot decouple the information on refractive index and thickness of thin films, simultaneous spectroscopy of multiple SP and HW modes allows to independently determine both these parameters and an even more detailed profile of hydrogel film density can be assessed. In general, thicker and denser hydrogel films support a higher number of modes with different distribution of the field intensity. Beines *et al.* used a reversed Wenzel-Kramers-Brillouin (WKB) approximation for determining the hydrogel density gradients from reflectivity spectra with a series of HW mode resonances. They observed photo-cross-linked PNIPAAM-based hydrogel films with a thickness of several micrometers and showed that the maximum density occurs at the inner interface and that the density continuously decreases to the out interface with water (see Figure 11.9b).

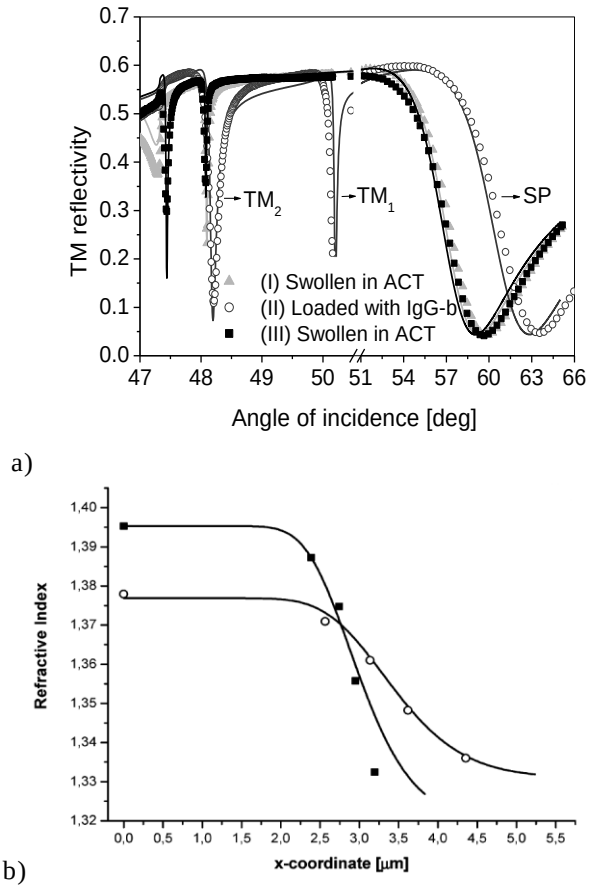

Figure 11.9 (a) Reflectivity spectra measured for the hydrogel film before (squares) and after (triangles) coupling of IgG molecules to 2 μm thick PNIPAAM-based gel. (Reproduced with permission from [46]). (b) WKB analysis of the refractive index profile for denser PNIPAAM-based hydrogel films. (Reproduced with permission from [22]).

The probing hydrogel films with two modes exhibiting different profiles of the electromagnetic field (e.g., coupled LRSPs [60] or LRSP and HW [32], as seen in

Figure 11.5 and Figure 11.8b) allows to determine thickness d_h and average refractive index n_h of a thin hydrogel film. Fresnel equations are typically used for fitting the measured reflectivity spectra in which the hydrogel density is approximated by using the "box model." In this model, the dependence of the refractive index perpendicular to the surface $n(x)$ is assumed to be the following function of the distance from the sensor surface:

$$n(x) = n_d + (n_h - n_d)H(d_h - x), \tag{11.5}$$

where x is the coordinate with the axis perpendicular to the sensor surface ($x = 0$ is the position at the interface between the metal and hydrogel) and H is the Heaviside step function. For a small refractive index n_h of a hydrogel, its surface mass density Γ can be calculated as:

$$\Gamma = (n_h - n_d) \times d_h \times \frac{\partial c}{\partial n_h}, \tag{11.6}$$

where the coefficient $\partial n_h / \partial c \sim 0.2$ mm^3 mg^{-1} relates changes in the refractive index and concentration of organic materials in the gel (e.g., polymer or proteins). On the basis of effective medium theory, the polymer volume fraction f of the swollen hydrogel is equal to:

$$f = \frac{(n_h^2 - n_d^2)(n_{h-dry}^2 + 2n_d^2)}{(n_h^2 + 2n_d^2)(n_{h-dry}^2 - n_d^2)} \tag{11.7}$$

where $n_{h\text{-}dry}$ is the refractive indices of the hydrogel in dry state.

11.3.5 Investigation of structured gels

Patterning for hydrogels is increasingly important in applications such as cell culturing, development of scaffolds for tissue engineering, and high-throughput assay platforms with microarray detection format. To date, numerous methods for structuring of hydrogels on a surface were developed including those based on microfluidics [65], photolithography [57, 66, 67] or soft-lithography-based techniques [68, 69].

SP resonance imaging (SPRi) is a label-free method that allows visualizing spatial distribution of polymers and biomolecules on metallic surfaces [70]. As shown in Fig. 11.11a, a large-diameter light beam is coupled to a high-refractive-index prism and SPs are excited at its base by using the ATR method with Kretschmann configuration. The angle of incidence of the excitation light beam, θ, is set to an edge of an SPR dip with a high slope $\partial R / \partial \theta$ (see Figure 11.8a). As the SPR dip shifts with a refractive index, the coupling strength to SPs at a given angle of incidence varies across the sensor chip with a different density or thickness of a hydrogel film. Therefore, the intensity of a reflected light beam is

modulated by the hydrogel structure and can be observed by its imaging at a spatially sensitive detector such as a charge-coupled device (CCD). Among other applications, SPRi was employed for the investigation of arrays of hydrogel spots. As illustrated in Fig. 11.11b, the Liedberg group applied SPRi for the characterization of a gradient HEMA microarray hydrogel that served as a binding matrix for interaction analysis of proteins [69].

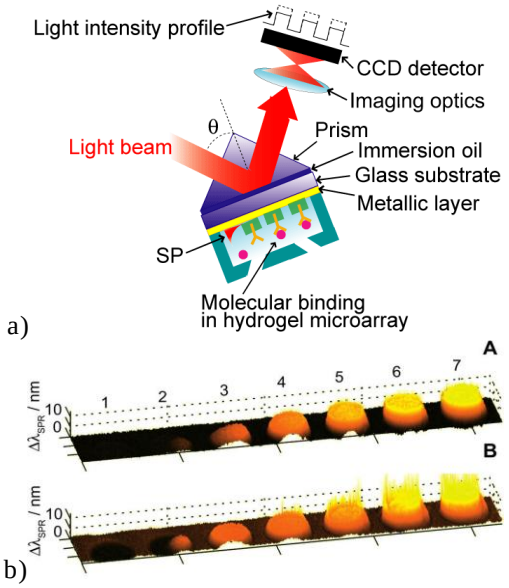

Figure 11.10 (a) Typical implementation of SPRi and (b) acquired image showing an array of hydrogel spots with increasing density before (A) and after (B) affinity biomolecular binding. (Reproduced with permission from [69]).

Another optical technique facilitated for investigation of periodically patterned hydrogel films is SP-enhanced diffraction (see Fig 11.12a). Zhang *et al.* used a periodically modulated photo-cross-linkable hydrogel film on the SPR sensor surface for studying its responsive properties by measuring the diffraction intensity [67]. As the collapse of the hydrogel triggered by an external stimulus leads to an increase in the refractive index contrast on a grating, it can be observed from the enhanced diffraction efficiency of the grating (Fig. 11.12b). The major advantage of this technique is the self-referencing, that is, the method is not sensitive to variations in a bulk solution upon the swelling/ collapse of a gel. Let us note that images acquired by SPR imaging and the SP-enhanced diffraction angular spectrum are related to each other through Fourier transform.

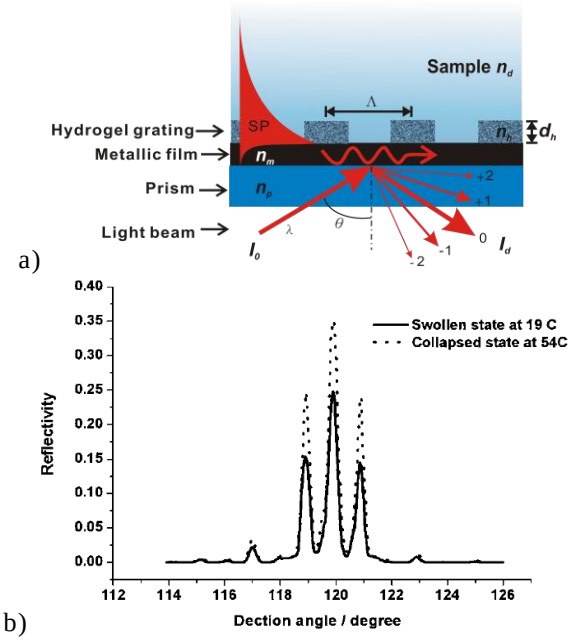

Figure 11.11 (a) SP-enhanced diffraction for the investigation of periodically patterned hydrogel films. (b) Example of the diffraction efficiency spectrum measured from a collapsed (dotted line) and swollen (solid line) gel. (Reproduced with permission from[67]).

11.4 Mass Transport and Affinity Binding of Analyte in a Gel

In the majority of evanescent wave affinity biosensors, the analyzed liquid sample is flowed through a flow-channel over a solid sensor surface with attached biomolecular recognition elements. As shown in Fig. 11.13, analyte molecules are captured on a sensor surface with biomolecular recognition elements and subsequently the binding events are converted to a sensor signal by a transducer. The flow velocity of a liquid sample in a flow-channel is zero at the surface (due to the viscosity of the liquid) and exhibits a parabolic profile in a flow-channel (see Figure 11.12). For a surface coated with a hydrogel binding matrix, the liquid flow penetrates into the gel only to a very small distance that scales with the gel mesh size [71]. Therefore, the transport of analyte molecules from a sample to the hydrogel binding matrix attached to a sensor surface is dominantly driven by diffusion.

A two-compartment model was developed to describe reactions on a surface with diffusion-driven analyte mass transfer [72]. In this model, the zero flow velocity at the surface is taken to account through a (hypothetical) unstirred layer with the thickness depending on a volumetric sample flow rate v and geometry of the flow-channel (i.e., on its depth h, length L, and width w). The diffusion rate

k_m of analyte molecules through the unstirred layer to and from the surface can be expressed as:

$$k_m = 1.378\left(\frac{v_{\max} D_s^2}{hL}\right)^{1/3}, \tag{11.8}$$

where D_s is the analyte diffusion coefficient in the bulk solution (sample) and v_{max} = 3/2 $v/(h \cdot w)$ is the flow velocity in the center of the flow-cell. For example, IgG molecules diffuse in an aqueous environment with the diffusion coefficient $D_s = 3\times10^{-5}$ mm^2 s^{-1} [31]. For a typical flow-channel with a depth of h = 100 µm, a length of L=10 mm, a width of w = 5 mm, and a flow velocity of v_{max} = 5 mm s^{-1}, the analyte molecules diffuse to the sensor surface at the rate of $k_m \sim 10^{-3}$ mm s^{-1}.

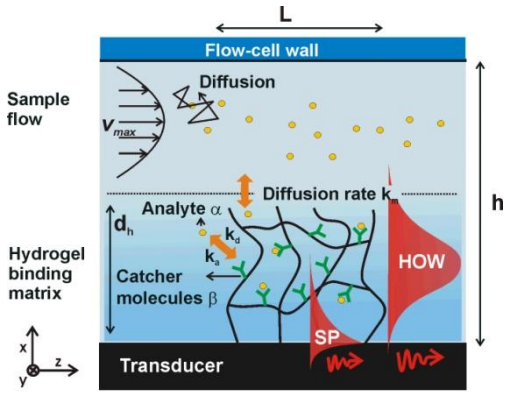

Figure 11.12 The scheme of a flow-cell channel with a hydrogel binding matrix attached to its bottom and analyte diffusing from a liquid sample.

11.4.1 Numerical model

Further, we introduce a numerical model for the analysis of the mass transport and affinity binding of the analyte to biomolecular recognition elements immobilized in a hydrogel on the sensor surface. This model was applied for the investigation of large-binding-capacity hydrogel matrices by Huang *et al.* [32], and it is based on the theory developed by Schuck *et al.* [73] for the evaluation of affinity binding constants by using SPR biosensor technology with a thin dextran brush binding matrix [72, 74].

In the model, we assume a reaction between analyte molecules A that are dissolved in a sample (at a concentration α) and catcher molecules B that are immobilized in a hydrogel (with a concentration β). The reaction fulfills the following conditions: i) all analyte and catcher molecules are identical, ii) one catcher molecule can bind only one analyte molecule, iii) analyte molecules react only with catcher molecules, and iv) each individual binding event is independent of the occupancy of other catcher molecules. The dynamic equilibrium of the reaction between α and β can be given as:

$$A + B \underset{k_d}{\overset{k_a}{\rightleftarrows}} AB, \tag{11.9}$$

where k_a and k_d are the association and dissociation rate constants, respectively.

A flow-cell geometry is depicted in Figure 11.12 and it is described by using Cartesian coordinates with the *x*-axis perpendicular to the surface and the *z*-axis parallel with the sample flow. Laminar flow of a sample through the flow-cell is assumed, which holds for the geometries with Reynolds number Re < 2100. Let us note that Reynolds number is equal to Re = (υ/ h)·0.998 mm^2s^{-1} for water at 20°C. In addition, the dependence of the concentration of free α and captured γ analyte on the *y* and *z* coordinates (with axis parallel to the sensor surface, respectively) is neglected. This approximation is valid for geometries in which Peclét number Pe = $v_{max}h^2/(D_sL)$ is large (Pe>>1). Under these conditions, the time and spatial dependence of the concentration of the captured analyte $\gamma(x,t)$ can be determined by solving the following set of partial differential equations (PDEs):

$$\frac{\partial \alpha}{\partial t} = D_g \frac{\partial^2 \alpha}{\partial x^2} - \frac{\partial \gamma}{\partial t}, \tag{11.10}$$

$$\frac{\partial \gamma}{\partial t} = k_a \alpha (\beta - \gamma) - k_d \gamma \cdot \tag{11.11}$$

The first equation (11.10) describes the diffusion of analyte α through the gel that is depleted due to the reaction with unoccupied catcher molecules. The second equation (11.11) takes into account the reaction between analyte molecules α and catcher molecules, β, forming a complex γ. In equation (11.10), the coefficient D_g states for the analyte diffusion coefficient in the gel. This coefficient is typically significantly lower than the one in a solution, owing to the presence of hydrogel polymer chains (see section 11.2.1)

The PDEs (11.10) and (11.11) can be solved for a defined set of boundary and initial conditions. For a sample flow that starts at t = 0, the following conditions (11.12)–(11.16) can be applied. Equations (11.12) and (11.13) defines the zero concentration of free α and captured γ analytes at t = 0, respectively. Equation (11.14) ensures that there are no sources of the analyte α in the gel at time t = 0, equation (11.15) defines the analyte flux through the inner hydrogel interface (i.e., the analyte cannot pass through the solid support on which gel is attached), and equation (11.16) describes that the analyte flux through the outer interface (with the sample) is driven by the diffusion rate k_m.

$$\alpha(x, t=0) = 0, \tag{11.12}$$

$$\gamma(x, t=0) = 0, \tag{11.13}$$

$$\frac{\partial \alpha}{\partial x}(x, t=0) = 0, \tag{11.14}$$

$$\frac{\partial \alpha}{\partial x}\left(x=0,t\right)=0\,, \tag{11.15}$$

$$\frac{\partial \alpha}{\partial x}\left(x=d_h,t\right)=\frac{k_m}{D_g}\left[\alpha_0-\alpha\left(d_h,t\right)\right]. \tag{11.16}$$

11.4.2 Profile of the analyte captured in the gel

When the concentration of bound analyte molecules is much smaller than that of catcher molecules, $\gamma<<\beta$, an analyte molecule diffusing through the gel becomes captured within a characteristic time $t_a = \ln(2)/(k_a\beta)$ that can be obtained from equation (11.11). Within time t_a, the analyte can diffuse into the functionalized gel up to a certain depth d_p that can be expressed on the basis of Fick's law as:

$$d_p=\sqrt{\frac{4D_g\ln\left(2\right)}{k_a\beta}}\,. \tag{11.17}$$

For the analyte binding after longer times or from samples with high concentration α_0, the reaction at binding sites within depth d_p reaches equilibrium and the analyte binding gradually shifts deeper into the hydrogel toward the solid support.

For the purpose of illustration, results obtained from the model are further compared with an experiment described by Huang *et al.* [32]. Analyte molecules (IgG) were diffused into a NIPAAm-based hydrogel film modified by catcher molecules (a-IgG) with parameters summarized in Table 11.1. For simplicity, a hydrogel with constant density of polymer chains and immobilized catcher molecules concentration β perpendicular to the surface was assumed ("box model").

Table 11.1 Values used in a numerical model

Association rate constant	$k_a = 6.5\times10^{4}$ M^{-1} s^{-1}
Dissociation rate constant	$k_d = 4.5\times10^{-5}$ mm^2 s^{-1}
Analyte diffusion coef. in hydrogel	$D_g = 10^{-6}$ mm^2 s^{-1}
Analyte diffusion coef. in sample	$D_b = 3\times10^{-5}$ mm^2 s^{-1}
Polymer volume content	f~0.1
Concentration of BREs	β = 90 μM
Thickness	d_h = 2 μm
Flow cell geometry	L = 8 mm, h = 0.3 mm, w = 5 mm
Flow rate	υ = 8.4 mm^{3}s^{-1}
Reynolds number	Re = 28
Peclét number	Pe = 3100

Figure 11.13a shows calculated spatial dependence of the concentration of the captured analyte γ on the concentration of the free analyte in a sample, α_0, after a 10-minute flow of a sample. The numerical model shows that the analyte binding occurs preferably in the outer hydrogel slice for small concentrations of the analyte in a sample, α_0 < 10 nM. The thickness of the slice agrees well with the

diffusion penetration depth of d_p = 0.7 μm obtained from equation (11.17). For higher concentrations of free analyte, α_0 > 0.1 μM, the majority of binding sites become occupied $\gamma \rightarrow \beta$ within the depth d_p and binding events gradually shift deeper in the gel with an increasing concentration α_0.

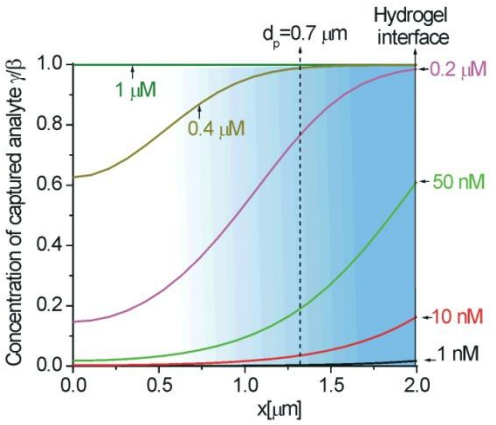

a)

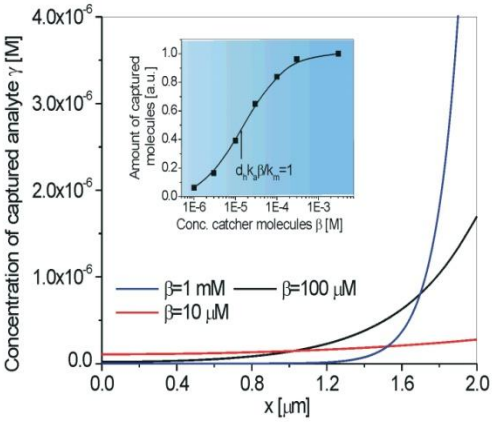

b)

Figure 11.13 Profile of the concentration of the captured analyte in a hydrogel matrix after a 10 min flow of a sample (a) with the analyte concentration α between 1 nM and 1 μM for a fixed concentration of catcher molecules, β = 90 μM; and (b) profile of the concentration of the captured analyte in a hydrogel for a fixed concentration of analyte in a sample, α_0 = 1 nM, and the concentration of catcher molecules, β, from 10 μM to 1 mM. The inset shows the dependence of the amount of the captured analyte on the concentration of catcher molecules, β.

Figure 11.13b shows a comparison of $\gamma(x)$ after 10 minutes flow of a sample with a low analyte concentration (α_0 = 1 nM) and the concentrations of catcher molecules, β, varied between 10 μM and 1 mM. It reveals that for hydrogels with low loading with catcher molecules (low binding capacity), the distribution of captured molecules $\gamma(x)$ is more homogenously distributed through the hydrogel matrix. For the high concentration β (large binding capacity), the analyte binding

occurs preferably in vicinity to the outer hydrogel interface, owing to a decreased diffusion penetration depth d_p.

An important observation is shown by the inset graph in Figure 11.13b. It reveals that increasing the binding capacity of the hydrogel above a certain value does not provide enhanced amount of captured molecules that become limited by the finite diffusion rate k_m. The effect of diffusion-limited mass transport on the analyte binding kinetics is typically quantified by using Darmköhler number that can be described for a studied hydrogel binding matrix as:

$$Da = \frac{d_h \beta k_a}{k_m}. \tag{11.18}$$

For a small Darmköhler number, Da<<1, the amount of the captured analyte linear increases with β and when Darmköhler number becomes large, Da>>1, it reaches a plateau. As seen in the inset of Figure 11.13b, the total amount of bound analyte molecules (calculated by integrating γ(x) through the hydrogel from $x = 0$ to d_h) converges to $k_m \alpha_0 \Delta t$ when the concentration of catcher molecules, β, is larger than 15 μM for which Da = 1.

11.4.3 Design of a hydrogel matrix

In an evanescent wave biosensor with a 3D binding matrix, the sensor response is proportional to the overlap of the field intensity of the probing wave, $|E(x)|^2$, and the distribution the of captured analyte, $\gamma(x)$:

$$S \propto \int_o^{d_h} |E(x)|^2 \gamma(x) dx \tag{11.19}$$

This equation holds for both biosensors detecting an analyte through binding-induced refractive index changes (refractometric) and via chromophore labels (fluorescence spectroscopy based). For refractometric biosensors, equation (11.19) can be derived from, for example, perturbation theory [75]. For fluorescence spectroscopy–based detection, the fluorescence light intensity is proportional to the excitation rate, which is (for randomly oriented chrompohores far from saturation) proportional to $|E(x)|^2$ at the absorption wavelength [60].

Figure 11.15 shows a comparison of the fluorescence signal simulated by using equation (11.19) with that measured after the binding of the target in a matrix with thickness d_h between 64 nm and 1440 nm, as reported by Huang *et al.* [32]. They employed a model immunoassay and the hydrogel binding matrix was probed with an LRSP mode exhibiting the penetration depth of $L_p/2$ = 460 nm. This data reveals that for the binding from a sample with a large analyte concentration, α_0 = 1.3 μM, the sensor response gradually increases with the thickness d_h and saturates when $d_h > L_p/2$. For a small analyte concentration α_0 = 0.67 pM, the maximum fluorescence signal is observed for the hydrogel thickness d_h between 130 nm and 330 nm and for larger thicknesses d_h the signal rapidly decreases. By comparing the experimental and theoretical dependence in Figure

11.14b, Huang *et al.* estimated the diffusion penetration depth for used surface architecture as d_p~400 nm, which is close to the optimum hydrogel thickness d_h.

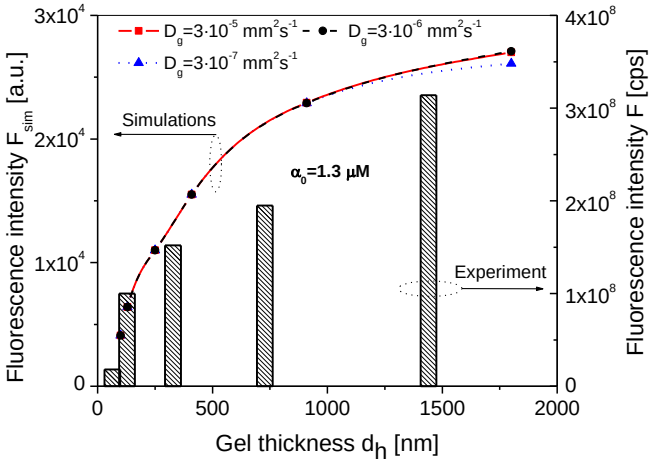

a)

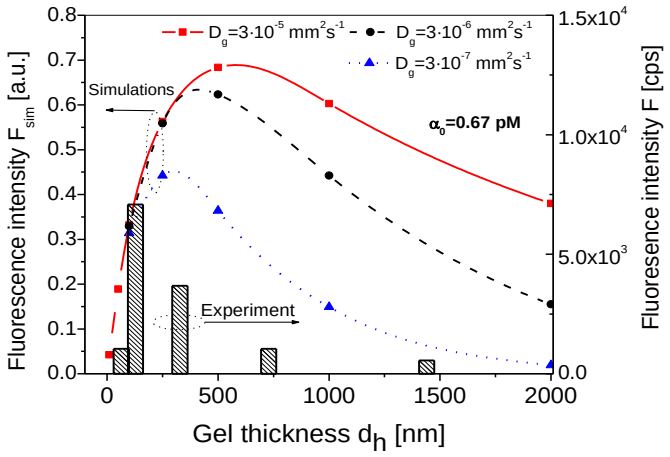

b)

Figure 11.14 The comparison of simulations (left axis) and measured (right axis) dependence of the fluorescence signal F on thickness of a hydrogel binding matrix, d_h. The hydrogel matrix was probed by LRSP mode after the 30-minute flow of a-IgG dissolved in a sample at (a) a low concentration of α_0 = 0.67 pM and (b) high concentration of α_0 = 1.3 μM. Diffusion coefficients in the gel of D_g = 3×10^{-5} mm^{2}s^{-1} (black ■), D_g = 3×10^{-6} mm^{2}s^{-1} (red ●), and Dg = 3×10^{-7} mm^{2}s^{-1} (blue ▲) were assumed. (Reprinted with permission from Huang *et al.* [32].)

The above-presented data illustrates that for maximizing the sensitivity of an evanescent wave affinity biosensor with a 3D hydrogel binding matrix for detection of trace amounts of molecular analytes, a delicate design of the sensor surface architecture needs to be carried out. The herein-presented model provides leads on how the interplay of key parameters, including the profile of a

probing wave $|E(x)|^2$, diffusion characteristics of an analyte to and through a gel, concentration of catcher molecules in the gel, β, and affinity binding rate constants k_a and k_d, affects the biosensor performance characteristics.

1.5 Biosensor Implementations

In this section, an overview of implementations of evanescent wave biosensors with a hydrogel binding matrix is presented. Representative examples of different biosensor schemes with molecular imprinted hydrogels, responsive gels modified with enzymes and biosensors relying on nucleic acids and immunoassays are introduced and their performance characteristics are discussed. Let us note, that this chapter does not provide a complete review of this topic, rather, interesting approaches were selected for the sake of illustration as summarized in Table 11.2.

1.5.1 Molecular imprinted hydrogel-based biosensors

Molecular imprinted hydrogels have attracted a great deal of attention over the last years [47, 48], and we witnessed the development of numerous biosensor schemes based on such materials. The majority of applications were carried out for refractometric-based detection of low-molecular-weight analytes relevant to medical diagnostics and environmental monitoring. Hydrogel-based imprinted matrices with responsive properties were shown to allow enhancing the sensitivity through binding-induced collapse or swelling that is associated with stronger refractive index changes and thus can be detected more accurately.

Willner *et al.* [76] developed a molecular imprinted acrylamide-acrylamidophenylboronic acid copolymer (AMPBA-AA) hydrogel for detection of β-nicotinamide adenine dinucleotide (NAD^+), β-nicotinamide adenine dinucleotide phosphate ($NADP^+$), and their reduced forms. As shown in Figure 11.15, SPR was employed for the detection of this important coenzyme of anabolic reactions. This approach took advantage of enhancing the refractive index changes associated with the analyte binding–induced swelling of the gel and allowed detection of $NADP^+$ and NADPH in the concentration range of 1 μM to 1 mM.

A way to further enhance the analyte binding-induced refractive index changes was pursued through the incorporation of metallic nanoparticles into molecular imprinted hydrogels [77], [78]. In such materials, stronger refractive index changes are observed upon the swelling or collapse of a gel, owing to distance-dependent localized surface plasmon resonance (LSPR) accompanied with near field coupling between individual nanoparticles. For instance, an LSPR sensor for detection of dopamine (important neurotransmitter) was developed by using

imprinted hydrogel, which consisted of acrylic acid (AA), N-isopropylacrylamide (NIPAAm), and N,N'-methylenbisacrylamide (MBS) [78].

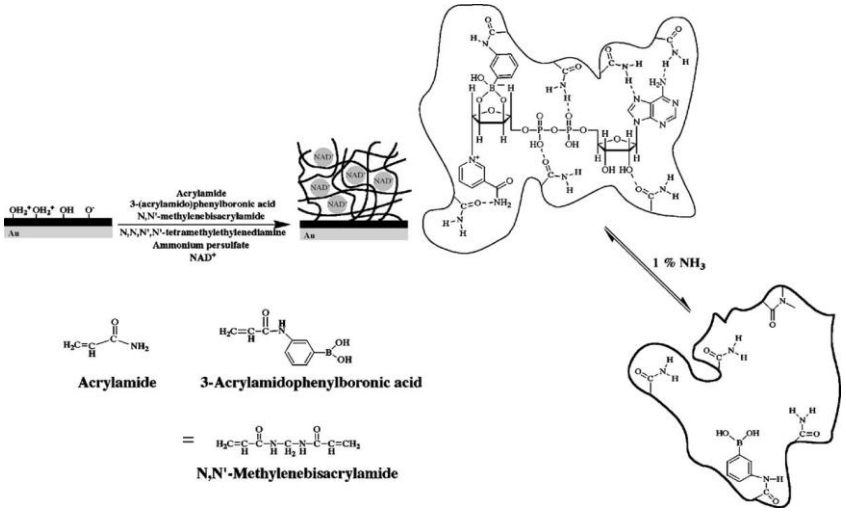

Figure 11.15 $NADP^+$/ NADPH cofactors-imprinted AMPBA-AA copolymer on an Au-coated glass for SPR-based detection. (Reproduced with permission from [76]).

Besides compact hydrogel films, molecular imprinted hydrogel particles can be used for the construction of a binding matrix. Lavine *et al.* employed such a surface architecture for the detection of theophylline [79]. They used polyN-(N-propyl)acrylamide (polyNNPA) nanoparticles with diameter of 300 nm tethered on a gold surface of an SPR sensor for detection of this methylxanthine drug. The binding of theophylline increased the phase transition temperature and hydrophilicity of the hydrogel. The associated decrease in the refractive index due to the theophylline capture was subsequently detected by SPR. The sensor showed specific detection of theophilline at concentrations above 10 µM.

1.5.2 Enzyme-based biosensors

Enzyme recognition elements were immobilized into a responsive hydrogel to simultaneously act as specific binding sites and means for amplification of the sensor signal. Typically, the analyte binding triggers a catalytic reaction, which leads to variations of responsive hydrogel matrix characteristics through, for example, a pH change. The enzyme reaction–induced collapse or swelling of a gel is subsequently converted to a sensor signal.

Bagal *et al.* developed a sucrose biosensor based on a hydrogel binding matrix that was composed from agarose-guar gum biopolymer, acid invertase, and glucose oxidase (GOx) [24]. This material was attached to a single-mode glass

optical waveguide. On the basis of the detection of the refractive index changes ascribed to the presence of sucrose in the hydrogel binding matrix with the thickness of 12 μm, the monitoring of waveguide attenuation provided rapid detection time of 110 seconds and a limit of detection as low as 25 pM.

A waveguide structure with a 1 μm thick sol-gel matrix was employed for the absorption and fluorescence spectroscopy–based detection of glucose by Zourob *et al.* [80]. The sol-gel matrix was modified with GOx and a fluorescent ruthenium complex that was sensitive to pH changes. The monitoring of glucose in a sample was pursued by the measuring of fluorescence quenching of ruthenium complex due to its protonation at excited state upon the release of gluconic acid by the bio-oxidation of glucose. The sensor demonstrated the limit of detection of 3 μM.

Another type of enzyme reaction–based transducing was reported by using "smart" hydrogel/ nanoparticles composites by the Minko group [81, 82]. These biosensors rely on the distance-dependent interaction of metal nanoparticles (see Figure 11.16). Through variations in the swelling/ collapse of the hydrogel host, embedded nanoparticles were dragged closer to or further from each other, which resulted in a modulation of LSPR. For instance, 20–25 nm thick alginate-gelatin film with encapsulated silver nanoparticles was deposited on a solid surface with silver islands. This system was demonstrated to respond to swelling variations of the film due to pH changes that were caused by the biocatalytic reaction of GOx. Endo *et al.* [83] used similar detection principle with a stimuli-responsive hydrogel-silver nanoparticles composite, consisting of acrylamide (AAm), bisacrylamide (bis-AAm), and PVP-coated silver nanoparticles.. The sensor relied on the formation of a reduced flavin adenine dinucleotide (FAD) anion, gluconic acid and hydrogen peroxide upon glucose turnover, which resulted in the swelling of hydrogel and degradation of silver nanoparticles associated with drastc LSPR changes [83]. On the basis of this reaction, the LSPR-based specific detection glucose at a concentration as low as 10 pM was achieved.

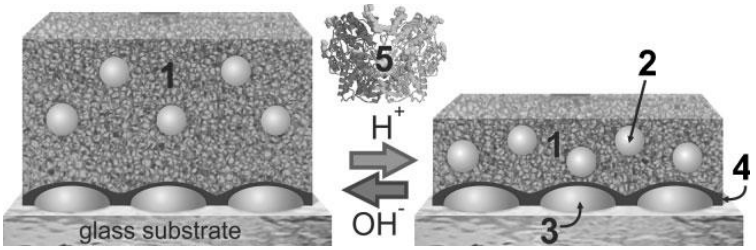

Figure 11.16 Plasmonic sensing device consisting of an ultrathin alginate-gelatin gel film (1) with silver nanoparticles (2) immobilized on silver nanoislands (3) via a PGMA layer (4). The film undergoes a reversible swelling transition in response to pH changes caused by the biocatalytic reaction of GOx (5) and glucose. (Reproduced with permission from [82]).

1.5.3 Nucleic acid–based biosensors

Hydrogel matrices were implemented for the detection of DNA analytes by using SPR and fluorescence spectroscopy by Nilsson's group [84, 85]. A water-soluble polythiophene polymer composed of poly(3-[(S)-5-amino-5-carboxyl-3-oxapentyl]-2,5-thiophenylene hydrochloride) (POWT) with zwitterionic peptide-like side chains was reacted with the single stranded probe DNA (ssDNA) via electrostatic and hydrogen bonding [85]. The zwitterionic side chains carry serine carboxylic groups with a p*Ka* of 2.19 and an amino group with a p*Ka* of 9.21 which are responsible for pH-dependent conformational transitions in the gel [86] (see Fig. 11.18a). This material aggregates to dense and straightened structure upon the incorporation of ssDNA probes (see Fig. 11.18b). After the hybridization with complementary target DNA strands forming a double stranded DNA (dsDNA), separation of polymer chains occurs which can be detected by SPR [86].

In addition, the POWT exhibits fluorescence properties that are sensitive to electrostatic interactions and hydrogen bonds between the polymer chains and other molecules. Nilsson *et al.* have shown that the POWT polymer emits fluorescence light at a longer wavelength when the net charge of the polymer side chains becomes more negative [86]. An introduced negatively charged ssDNA interacts electrostatically with the positively charged amino groups on polymer chains and subsequently forms hydrogen bonds with the polymer amino and carboxyl groups. Thus, the POWT shows a red-shift and a decrease of the peak fluorescence intensity upon the incorporation of ssDNA probes. After the capture of target DNA analyte, the hydrogen bonding between the polymer chain and the ssDNA is disrupted which leads to a separation of the polymer chains with less negatively charged and coil backbone [85] (see Fig. 11.18b). Therefore, the intensity of the emitted light is increased and blue-shifted. This method allowed detection of DNA at a concentration as low as 6.7 nM.

Another type of a novel nucleic acid–based biosensor with aptamer cross-linked polyacrylamide (PAA) hydrogel was developed by Tan's group for the detection of small molecules, such as adenosine [87] and cocaine [88]. Used hydrogels were modified by two different DNA strands that were cross-linked by an aptamer linker. The specific reaction of target analyte with the aptamer linker resulted in a reducing of hydrogel cross-linking density accompanied with gel dissolution and release of embedded Au nanoparticles or enzymes. Their activity can be optically detected and allowed detecting of cocaine at concentrations below 1 μM within 10 minutes [88].

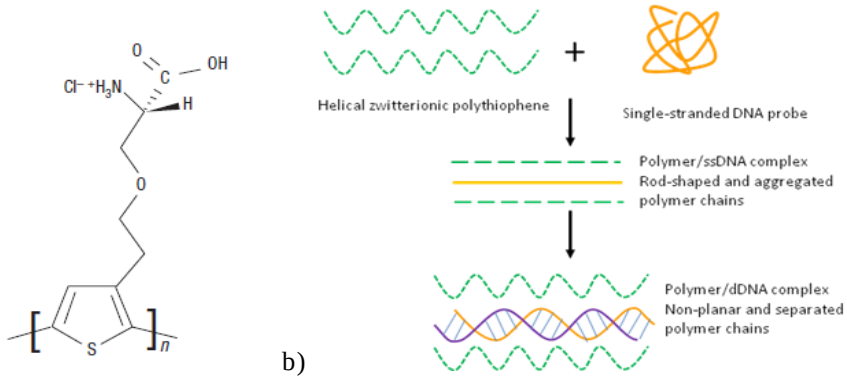

Figure 11.17 (a) The repeated unit of POWT and (b) the formation of POWT/ DNA complexes. Geometrical changes of POWT (dotted lines) on addition of ssDNA (solid lines) and dsDNA (helical structure). (Reproduced with permission from [85]).

1.5.4 Immunoassay-based biosensors

Immunoassays represent an established method for detection of molecular analytes, owing to their versatility and availability of a wide range of antibodies with high affinity. Biosensor schemes with antibodies immobilized in hydrogel films take advantage of increased binding capacity and lower steric hindrance offered by their open (3D) structure. Three representative examples of immunoassay-based detection of target molecules by label-free techniques relying on the monitoring of binding-induced refractive index changes and by fluorescence spectroscopy are presented in the following section.

Liedberg *et al.* employed an SPRi for the investigation of a gradient hydrogel matrix composed of PEG methacrylate ($PEG_{10}MA$) and 2-hydroxyethyl HEMA prepared in microarray format [57]. Biospecific interaction between two affinity pairs of human serum albumin (HSA) / anti-HSA antibodies and calmodulin (CaM) / calmodulin binding domain (CBD) was studied as a function of thickness and composition of the matrix. Due to the low porosity of the hydrogel matrix, CaM with a low molecular weight was shown to diffuse and interact throughout the entire hydrogel matrix carrying CBD protein. HSA diffusion into the gel was hindered due to its larger size and thus reacted only on the top of the gel. It was demonstrated that the SPRi sensitivity for the detection of CaM depends on the thickness of the hydrogel, and the highest sensitivity for detection of CaM was achieved for the thickness of $PEG_{10}MA$/ HEMA hydrogel matrix of 70 nm.

Wang *et al.* have used a highly swollen PNIPAAm-based hydrogel with a thickness around 2 μm for the construction of a label-free immunosensor based on hydrogel optical waveguide spectroscopy (HOWS) [23]. Owing to low polymer volume content of $f \sim 0.1$, even larger molecules such as IgG molecules diffused rapidly into the gel and reacted with immobilized biomolecular capture antibodies. As Figure 11.18 shows, the swollen hydrogel served simultaneously

as a binding matrix and an optical waveguide and thus full overlap of the probing electromagnetic field with the matrix was achieved. In comparison with regular SPR with monolayer biointerfaces architecture, the HOWS detection method provided an order-of-magnitude-improved resolution in the refractive index measurements due to the narrower resonance associated with the excitation of HW modes (see Figure 11.18). In a model immunoassay experiment, a five-folder lower limit of detection for IgG molecules was demonstrated for HOWS with respect to the regular SPR method. Larger sensitivity enhancements are expected for detection of smaller molecules that diffuse faster to the gel and for which the HOWS biosensor scheme can fully take advantage of its large binding capacity.

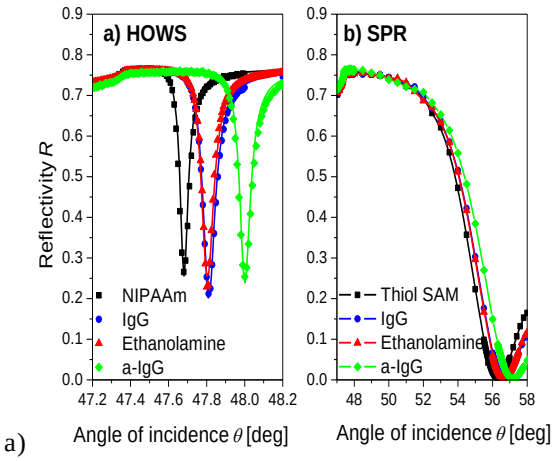

a)

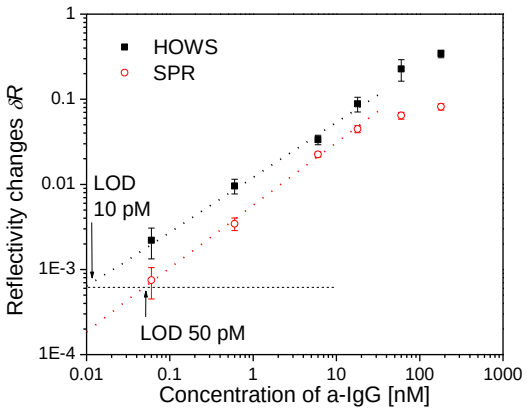

b)

Figure 11.18 (a) Reflectivity spectra measured for HOWS with approximately a 2 μm thick hydrogel binding matrix and regular SPR with thiol SAM surface architecture upon coupling of biomolecular recognition elements (circles, IgG) and after-affinity binding of the target analyte (diamonds, a-IgG). (b) Comparison of LOD for HOW and SPR by using a model immunoassays experiment. (Reproduced with permission from [23]).

Wang *et al.* have developed an immunosensor for detection of free prostate specific antigen (f-PSA) with a highly swollen photo-cross-linkable carboxymethyl dextran hydrogel binding matrix that was probed by LRSP modes (see Fig. 11.20a). They employed a sandwich assay with a hydrogel matrix modified by capture antibodies, followed by the binding of target analyte and decoration of the captured analyte molecules with detection antibodies labeled with a chromophore. The thickness of the hydrogel was close to 1 μm and was similar to the penetration depth of the probing LRSP mode. In this method, strong electromagnetic field intensity provided by the excitation of LRSPs served for the strong excitation of chromophore labels that was directly translated to the enhanced fluorescence signal [15].

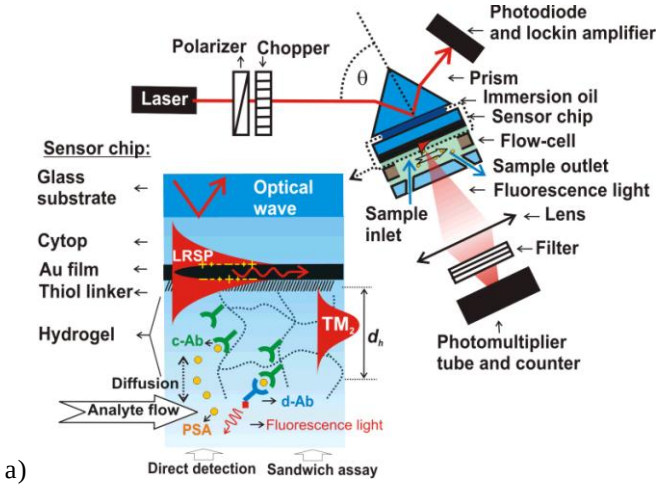

a)

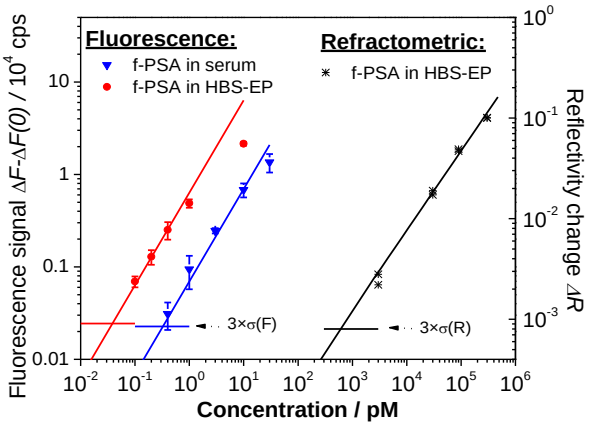

b)

Figure 11.19 Optical setup for the excitation of LRSPs on the sensor surface with a PCMD hydrogel binding matrix and the f-PSA sandwich immunoassay. (b) Calibration curve for the direct and fluorescence-based detection of f-PSA in a buffer and human serum. (Reproduced with permission from [15]).

As seen in Fig. 11.20b, the biosensor enabled detection of f-PSA with the limit of detection at a low femtomolar range. This limit of detection was about four orders of magnitude lower than that observed for direct detection of f-PSA (through measuring refractive index changes of the gel by spectroscopy of LRSP). In addition, the performance of fluorescence-based readout was less affected by the nonspecific sorption and allowed the analysis of f-PSA in human serum.

Table 11.2 Overview of hydrogel biosensors based on evanescent wave optics

Recognition element	Material	Method	Thickness d_h	Analyte	LOD (sample)	Ref.
MIP	P2VP-AuNPs	LSPR	31 nm	cholesterol	n.a. (chloroform)	[20]
	AMPBA-AA	SPR	22 nm	$NAD(P)^+$ NAD(P)H	1 µM (buffer)	[76]
	AA-NIPAAm-MBS-AuNPs	SPR	~6 µm (dry)	dopamine	1 nM (water)	[78]
	polyNNPA	SPR	~300 nm	Theophylline	10 µM (buffer)	[79]
	MAA-EGDMA-AIBN-AuNPs	SPR	251nm	atrazine	5 pM (acetonitrile)	[89]
Enzyme	agaros-guar gum polysaccharide	OWS	12 µm	sucrose	25 pM (buffer)	[24]
	agarose co-polymer	OWS	1 µm	paraoxon	6 nM (buffer)	[80]
	agarose co-polymer	OWS-Fluorescence	1 µm	glucose	3 µM (buffer)	[80]
	alginate-gelatin-AgNPs	LSPR	20 nm (dry)	glucose	0.1 mM (buffer)	[82]
	AAm-bisAAm-AgNPs	LSPR	~1 mm	glucose	10 pM (buffer)	[83]
Nucleic acid	POWT	SPR	8 nm (dry)	DNA	n.a. (buffer)	[84]
	aptamer-PAA	LSPR	n.a.	adenosine	n.a. (buffer)	[87]
	aptamer-PAA	LSPR	n.a.	cocanie	n.a. (buffer)	[88]
Immuno-assay	CMD	LR-SPR	~1µm	f-PSA	0.68 nM (buffer)	[15]
	CMD	LRSP-FS	~1µm	f-PSA	34 fM (buffer) 330 fM (human serum)	[15]
	PNIPAAm	HOWS	~2µm	IgG	10 pM (buffer)	[23]
	PEG_{10}MA-HEMA	SPRi	5-45 nm	HSA and calmodulin	n.a. (buffer)	[57]

1.6 Conclusion and Outlook

Hydrogel materials employed in biosensors allowed to impressively advance their performance and push these technologies toward important application

fields such as medical diagnostics and environmental monitoring. Particularly, we witnessed the development of new materials with excellent resistance against nonspecific sorption from complex samples, such as blood serum, and advanced recognition characteristics through incorporation of specific moieties by molecular imprinting or through coupling of biomolecules. Evanescent wave optics provides valuable means for both biosensor implementations and observation of thin hydrogel films. We expect that future biosensor technologies will increasingly take advantage of "smart" hydrogels with responsive properties enabling increasing their sensitivity and implementing detection schemes suitable for miniature biosensors with simplified readout. In addition, recognition of target analytes based on molecular imprinting will play an increasingly important role. In conjunction with optical detection methods, advances in such large binding capacity materials hold potential to deliver urgently needed biosensor tools for direct label-free detection of low-molecular-weight molecules such as drugs in medical diagnostics or pollutants in environmental monitoring. For such analytes, currently established technologies, including immunoassay-based SPR, lack sensitivity and long-term stability.

11.7 Acknowledgments

Partial support for this work was provided by Deutsche Forschungsgemainschaft (KN 224/ 18-1, Schwerpunktprogramm "Intelligente Hydrogele", SPP 1259) and ZIT, Center of Innovation and Technology of Vienna and NILPlasmonics project within the NILAustria cluster (www.NILAustria.at).

References

1. Nicodemus, G. D. and Bryant, S. J. (2008). Cell encapsulation in biodegradable hydrogels for tissue engineering applications, *Tissue Engineering Part B: Reviews*, **14**, pp. 149..165.
2. Shoichet, M. S. (2010). Polymer scaffolds for biomaterials applications, *Macromolecules*, **43**, pp. 581..591.
3. Slaughter, B. V., Khurshid, S. S., Fisher, O. Z., Khademhosseini, A. and Peppas, N. A. (2009). Hydrogels in regenerative medicine, *Advanced Materials*, **21**, pp. 3307..3329.
4. Hamidi, M., Azadi, A. and Rafiei, P. (2008). Hydrogel nanoparticles in drug delivery, *Advanced Drug Delivery Reviews*, **60**, pp. 1638..1649.
5. Hoare, T. R. and Kohane, D. S. (2008). Hydrogels in drug delivery: Progress and challenges, *Polymer*, **49**, pp. 1993..2007.
6. Bajpai, A. K., Shukla, S. K., Bhanu, S. and Kankane, S. (2008). Responsive polymers in controlled drug delivery, *Progress in Polymer Science*, **33**, pp. 1088..1118.
7. Gerlach, M. G. a. G. (2009) *Hydrogels for chemical sensors*, in *Hydrogel Sensors and Actuators*, G.A. Urban, Editor. Springer: Heidelberg. p. 165.
8. Richter, A., Paschew, G., Klatt, S., Lienig, J., Arndt, K. F. and Adler, H. J. P. (2008). Review on hydrogel-based pH sensors and microsensors, *Sensors*, **8**, pp. 561..581.

9. Tokarev, I. and Minko, S. (2009). Stimuli-responsive hydrogel thin films, *Soft Matter*, **5**, pp. 511..524.
10. Weiss, G. A. U. a. T. (2009) *Hydrogels for biosensors*, in *Hydrogel Sensors and Actuators*, G.A. Urban, Editor. Springer: Heidelberg. p. 197.
11. Davies, M. L., Murphy, S. M., Hamilton, C. J. and Tighe, B. J. (1992). Polymer membranes in clinical sensor applications. 3. hydrogels as reactive matrix membranes in fiber optic sensors, *Biomaterials*, **13**, pp. 991-999.
12. Murphy, S. M., Hamilton, C. J., Davies, M. L. and Tighe, B. J. (1992). Polymer membranes in clinical sensor applications. 2. the design and fabrication of permselective hydrogels for electrochemical devices, *Biomaterials*, **13**, pp. 979-990.
13. Yang, X. P., Pan, X. H., Blyth, J. and Lowe, C. R. (2008). Towards the real-time monitoring of glucose in tear fluid: Holographic glucose sensors with reduced interference from lactate and pH, *Biosensors & Bioelectronics*, **23**, pp. 899-905.
14. Ladet, S., David, L. and Domard, A. (2008). Multi-membrane hydrogels, *Nature*, **452**, pp. 76..79.
15. Wang, Y., Brunsen, A., Jonas, U., Dostalek, J. and Knoll, W. (2009). Prostate specific antigen biosensor based on long range surface plasmon-enhanced fluorescence spectroscopy and dextran hydrogel binding matrix, *Analytical Chemistry*, **81**, pp. 9625..9632.
16. Li, N., Liu, Z. Z. and Xu, S. G. (2000). Dynamically formed poly (vinyl alcohol) ultrafiltration membranes with good anti-fouling characteristics, *Journal of Membrane Science*, **169**, pp. 17..28.
17. Bakshi, A., Fisher, O., Dagci, T., Himes, B. T., Fischer, I. and Lowman, A. (2004). Mechanically engineered hydrogel scaffolds for axonal growth and angiogenesis after transplantation in spinal cord injury, *Journal of Neurosurgery-Spine*, **1**, pp. 322..329.
18. Guvendiren, M., Yang, S. and Burdick, J. A. (2009). Swelling-induced surface patterns in hydrogels with gradient crosslinking density, *Advanced Functional Materials*, **19**, pp. 3038..3045.
19. Tokarev, I., Tokareva, I. and Minko, S. (2008). Gold-nanoparticle-enhanced plasmonic effects in a responsive polymer gel, *Advanced Materials*, **20**, pp. 2730..2734.
20. Tokareva, I., Tokarev, I., Minko, S., Hutter, E. and Fendler, J. H. (2006). Ultrathin molecularly imprinted polymer sensors employing enhanced transmission surface plasmon resonance spectroscopy, *Chemical Communications*, **31**, pp. 3343..3345.
21. Ishihara, K., Kobayashi, M., Ishimaru, N. and Shinohara, I. (1984). Glucose induced permeation control of insulin through complexmembrane consisting of immobilized glucose oxidase and a poly(amine), *Polymer Journal*, **16**, pp.
22. Beines, P. W., Klosterkamp, I., Menges, B., Jonas, U. and Knoll, W. (2007). Responsive thin hydrogel layers from photo-cross-linkable poly(N-isopropylacrylamide) terpolymers, *Langmuir*, **23**, pp. 2231..2238.
23. Wang, Y., Huang, C. J., Jonas, U., Wei, T. X., Dostalek, J. and Knoll, W. (2010). Biosensor based on hydrogel optical waveguide spectroscopy, *Biosensors & Bioelectronics*, **25**, pp. 1663..1668.
24. Bagal, D. S., Vijayan, A., Aiyer, R. C., Karekar, R. N. and Karve, M. S. (2007). Fabrication of sucrose biosensor based on single mode planar optical waveguide using co-immobilized plant invertase and GOD, *Biosensors & Bioelectronics*, **22**, pp. 3072..3079.
25. Kuckling, D. (2009). Responsive hydrogel layers-from synthesis to applications, *Colloid. Polym. Sci.*, **287**, pp. 881-891.
26. Janshoff, A., Dancil, K. P. S., Steinem, C., Greiner, D. P., Lin, V. S. Y., Gurtner, C., Motesharei, K., Sailor, M. J. and Ghadiri, M. R. (1998). Macroporous p-type

silicon Fabry-Perot layers. Fabrication, characterization, and applications in biosensing, *Journal of the American Chemical Society*, **120**, pp. 12108-12116.

27. Lau, K. H. A., Tan, L. S., Tamada, K., Sander, M. S. and Knoll, W. (2004). Highly sensitive detection of processes occurring inside nanoporous anodic alumina templates: A waveguide optical study, *Journal of Physical Chemistry B*, **108**, pp. 10812..10818.
28. Feng, C. L., Zhong, X. H., Steinhart, M., Caminade, A. M., Majoral, J. P. and Knoll, W. (2007). Graded-bandgap quantum-dot-modified nanotubes: A sensitive biosensor for enhanced detection of DNA hybridization, *Advanced Materials*, **19**, pp. 1933..1936.
29. Kambhampati, D. K., Jakob, T. A. M., Robertson, J. W., Cai, M., Pemberton, J. E. and Knoll, W. (2001). Novel silicon dioxide sol-gel films for potential sensor applications: A surface plasmon resonance study, *Langmuir*, **17**, pp. 1169..1175.
30. Cameron, P. J., Jenkins, A. T. A., Knoll, W., Marken, F., Milsom, E. V. and Williams, T. L. (2008). Optical waveguide spectroscopy study of the transport and binding of cytochrome c in mesoporous titanium dioxide electrodes, *Journal of Materials Chemistry*, **18**, pp. 4304..4310.
31. Jossang, T., Feder, J. and Rosenqvist, E. (1988). Photon correlation spectroscopy of human IgG, *Journal of Protein Chemistry*, **7**, pp. 1573..4943.
32. Huang, C. J., Dostalek, J. and Knoll, W. (2010). Long range surface plasmon and hydrogel waveguide field-enhanced fluorescence biosensor with 3D binding matrix: on the role of mass transport, *Biosens. Bioelectron.*, **26**, pp. 1425-1431.
33. Hink, M. A., Griep, R. A., Borst, J. W., van Hoek, A., Eppink, M. H. M., Schots, A. and Visser, A. J. W. G. (2000). Structural dynamics of green fluorescent protein alone and fused with a single chain Fv protein, *Journal of Biological Chemistry*, **275**, pp. 17556-17560.
34. Raccis, R. (personal communication).
35. Sershen, S. R., Mensing, G. A., Ng, M., Halas, N. J., Beebe, D. J. and West, J. L. (2005). Independent optical control of microfluidic valves formed from optomechanicaly responsive nanocomposite hydrogels, *Advanced Materials*, **17**, pp. 1366..1368.
36. Satarkar, N. S., Zhang, W. L., Eitel, R. E. and Hilt, J. Z. (2009). Magnetic hydrogel nanocomposites as remote controlled microfluidic valves, *Lab Chip*, **9**, pp. 1773..1779.
37. Fuhrer, R., Athanassiou, E. K., Luechinger, N. A. and Stark, W. J. (2009). Crosslinking metal nanoparticles into the polymer backbone of hydrogels enables preparation of soft, magnetic field-driven actuators with muscle-like flexibility, *Small*, **5**, pp. 383..388.
38. Ostuni, E., Chapman, R. G., Holmlin, R. E., Takayama, S. and Whitesides, G. M. (2001). A survey of structure-property relationships of surfaces that resist the adsorption of protein, *Langmuir*, **17**, pp. 5605-5620.
39. Holmlin, R. E., Chen, X. X., Chapman, R. G., Takayama, S. and Whitesides, G. M. (2001). Zwitterionic SAMs that resist nonspecific adsorption of protein from aqueous buffer, *Langmuir*, **17**, pp. 2841-2850.
40. Prime, K. L. and Whitesides, G. M. (1991). Self-assembled organic monolayers-model systems for studying adsorption of proteins at surfaces, *Science*, **252**, pp. 1164..1167.
41. Chen, S. F., Zheng, J., Li, L. Y. and Jiang, S. Y. (2005). Strong resistance of phosphorylcholine self-assembled monolayers to protein adsorption: Insights into nonfouling properties of zwitterionic materials, *Journal of the American Chemical Society*, **127**, pp. 14473..14478.
42. Zhang, Z., Chen, S. F., Chang, Y. and Jiang, S. Y. (2006). Surface grafted sulfobetaine polymers via atom transfer radical polymerization as superlow fouling coatings, *Journal of Physical Chemistry B*, **110**, pp. 10799..10804.

43. Vaisocherova, H., Yang, W., Zhang, Z., Cao, Z. Q., Cheng, G., Piliarik, M., Homola, J. and Jiang, S. Y. (2008). Ultralow fouling and functionalizable surface chemistry based on a zwitterionic polymer enabling sensitive and specific protein detection in undiluted blood plasma, *Analytical Chemistry*, **80**, pp. 7894..7901.
44. Carrigan, S. D. and Tabrizian, M. (2005). Reducing nonspecific adhesion on cross-linked hydrogel platforms for real-time immunoassay in serum, *Langmuir*, **21**, pp. 12320..12326.
45. Masson, J. F., Battaglia, T. M., Davidson, M. J., Kim, Y. C., Prakash, A. M. C., Beaudoin, S. and Booksh, K. S. (2005). Biocompatible polymers for antibody support on gold surfaces, *Talanta*, **67**, pp. 918..925.
46. Aulasevich, A., Roskamp, R. F., Jonas, U., Menges, B., Dostalek, J. and Knoll, W. (2009). Optical waveguide spectroscopy for the investigation of protein-functionalized hydrogel films, *Macromolecular Rapid Communications*, **30**, pp. 872..877.
47. Byrne, M. E., Park, K. and Peppas, N. A. (2002). Molecular imprinting within hydrogels, *Advanced Drug Delivery Reviews*, **54**, pp. 149..161.
48. Byrne, M. E. and Salian, V. (2008). Molecular imprinting within hydrogels II: Progress and analysis of the field, *International Journal of Pharmaceutics*, **364**, pp. 188..212.
49. Guo, M. J., Zhao, Z., Fan, Y. G., Wang, C. H., Shi, L. Q., Xia, J. J., Long, Y. and Mi, H. F. (2006). Protein-imprinted polymer with immobilized assistant recognition polymer chains, *Biomaterials*, **27**, pp. 4381..4387.
50. Dickert, F. L. and Hayden, O. (2002). Bioimprinting of polymers and sol-gel phases. Selective detection of yeasts with imprinted polymers, *Analytical Chemistry*, **74**, pp. 1302..1306.
51. Guerreiro, A. R., Chianella, I., Piletska, E., Whitcombe, M. J. and Piletsky, S. A. (2009). Selection of imprinted nanoparticles by affinity chromatography, *Biosensors & Bioelectronics*, **24**, pp. 2740..2743.
52. Haupt, K. (2001). Molecularly imprinted polymers in analytical chemistry, *Analyst*, **126**, pp. 747..756.
53. Haupt, K. and Mosbach, K. (2000). Molecularly imprinted polymers and their use in biomimetic sensors, *Chemical Reviews*, **100**, pp. 2495..2504.
54. Löfås, S., Johnsson, B., Tegendal, K. and Rönnberg, I. (1993). Dextran modified gold surface for surface plasmon resonancesensor immunoreactivity of immobilized antibodies and antbody-surface interaction studies, *Colloids and Surfaces B: Biointerfaces*, **1**, pp. 83..89.
55. Su, X. D., Wu, Y. J., Robelek, R. and Knoll, W. (2005). Surface plasmon resonance spectroscopy and quartz crystal microbalance study of streptavidin film structure effects on biotinylated DNA assembly and target DNA hybridization, *Langmuir*, **21**, pp. 348-353.
56. Larsson, A. and Liedberg, B. (2007). Poly(ethylene glycol) gradient for biochip development, *Langmuir*, **23**, pp. 11319..11325.
57. Andersson, O., Larsson, A., Ekblad, T. and Liedberg, B. (2009). Gradient hydrogel matrix for microarray and biosensor applications: an imaging SPR study, *Biomacromolecules*, **10**, pp. 142-148.
58. Huang, C. J., Jonas, U., Dostalek, J., Knoll, W. (2009). Biosensor platform based on surface plasmon-enhanced fluorescence spectroscopy and responsive hydrogel binding matrix *Proceedings of SPIE*, **7356**, pp. 735625.
59. Sarid, D. (1981). Long-range surface-plasma waves on vary thin metal films, *Physical Review Letters*, **47**, pp. 1927..1930.
60. Dostalek, J. and Knoll, W. (2008). Biosensors based on surface plasmon-enhanced fluorescence spectroscopy, *Biointerphases*, **3**, pp. 12..22.

61. Wang, Y., Huang, C. J., Jonas, U., Wei, T. X., Dostalek, J. and Knoll, W. (2010). Biosensor based on hydrogel optical waveguide spectroscopy, *Biosens. Bioelectron.*, **25**, pp. 1663-1668.
62. Huang, C. J., Jonas, U., Dostalek, J., Knoll, W. (2009). Biosensor platform based on surface plasmon-enhanced fluorescence spectroscopy and responsive hydrogel binding matrix *Proc. SPIE*, **7356**, pp. 735625.
63. Dostalek, J., Roskamp, R. F. and Knoll, W. (2009). Coupled long range surface plasmons for the investigation of thin films and interfaces, *Sensor and Actuators B*, **139**, pp. 9..12.
64. Harmon, M. E., Jakob, T. A. M., Knoll, W. and Frank, C. W. (2002). A surface plasmon resonance study of volume phase transitions in N-isopropylacrylamide gel films, *Macromolecules*, **35**, pp. 5999..6004.
65. Hou, H. J., Kim, W., Grunlan, M. and Han, A. (2009). A thermoresponsive hydrogel poly(N-isopropylacrylamide) micropatterning method using microfluidic techniques, *Journal of Micromechanics and Microengineering*, **19**, pp. 6.
66. Revzin, A., Russell, R. J., Yadavalli, V. K., Koh, W. G., Deister, C., Hile, D. D., Mellott, M. B. and Pishko, M. V. (2001). Fabrication of poly(ethylene glycol) hydrogel microstructures using photolithography, *Langmuir*, **17**, pp. 5440..5447.
67. Zhang, N. and Knoll, W. (2009). Thermally responsive hydrogel films studied by surface plasmon diffraction, *Anal. Chem.*, **81**, pp. 2611-2617.
68. Kobel, S., Limacher, M., Gobaa, S., Laroche, T. and Lutolf, M. P. (2009). Micropatterning of hydrogels by soft embossing, *Langmuir*, **25**, pp. 8774..8779.
69. Zhou, Y., Andersson, O., Lindberg, P. and Liedberg, B. (2004). Reversible hydrophobic barriers introduced by microcontact printing: Application to protein microarrays, *Microchimica Acta*, **146**, pp. 193..205.
70. Scarano, S., Mascini, M. and Turner, A. P. F. (2010). Surface plasmon resonance imaging for affinity-based biosensors, *Biosensors & Bioelectronics*, **25**, pp. 957..966.
71. Milner, S. T. (1991). Hydrodynamic penetration into parabolic brushes, *Macromolecules*, **24**, pp. 3704..3705.
72. Edwards, D. A. (2001). The effect of a receptor layer on the measurement of rate constants, *Bulletin of Mathematical Biology*, **63**, pp. 301..327.
73. Schuck, P. (1996). Kinetics of ligand binding to receptor immobilized in a polymer matrix, as detected with an evanescent wave biosensor .1. A computer simulation of the influence of mass transport, *Biophysical Journal*, **70**, pp. 1230..1249.
74. Sikavitsas, V., Nitsche, J. M. and Mountziaris, T. J. (2002). Transport and kinetic processes underlying biomolecular interactions in the BIACORE biosensor, *Biotechnology Progress*, **18**, pp. 885..897.
75. Snyder, A. W. and Love, J. (1983) *Optical Waveguide Theory*. (Chapman and Hall, New York) pp.
76. Raitman, O. A., Chegel, V. I., Kharitonov, A. B., Zayats, M., Katz, E. and Willner, I. (2004). Analysis of NAD(P)(+) and NAD(P)H cofactors by means of imprinted polymers associated with Au surfaces: A surface plasmon resonance study, *Analytica Chimica Acta*, **504**, pp. 101..111.
77. Matsui, J., Akamatsu, K., Nishiguchi, S., Miyoshi, D., Nawafune, H., Tamaki, K. and Sugimoto, N. (2004). Composite of Au nanoparticles and molecularly imprinted polymer as a sensing material, *Analytical Chemistry*, **76**, pp. 1310..1315.
78. Matsui, J., Akamatsu, K., Hara, N., Miyoshi, D., Nawafune, H., Tamaki, K. and Sugimoto, N. (2005). SPR sensor chip for detection of small molecules using molecularly imprinted polymer with embedded gold nanoparticles, *Analytical Chemistry*, **77**, pp. 4282..4285.
79. Lavine, B. K., Westover, D. J., Kaval, N., Mirjankar, N., Oxenford, L. and Mwangi, G. K. (2007). Swellable molecularly imprinted polyN-(N-propyl)acrylamide particles for detection of emerging organic contaminants

using surface plasmon resonance spectroscopy, *Talanta*, **72**, pp. 1042..1048.

80. Zourob, M. and Goddard, N. J. (2005). Metal clad leaky waveguides for chemical and biosensing applications, *Biosensors & Bioelectronics*, **20**, pp. 1718..1727.
81. Stuart, M. A. C., Huck, W. T. S., Genzer, J., Muller, M., Ober, C., Stamm, M., Sukhorukov, G. B., Szleifer, I., Tsukruk, V. V., Urban, M., Winnik, F., Zauscher, S., Luzinov, I. and Minko, S. (2010). Emerging applications of stimuli-responsive polymer materials, *Nature Materials*, **9**, pp. 101..113.
82. Tokarev, I., Tokareva, I., Gopishetty, V., Katz, E. and Minko, S. (2010). Specific biochemical-to-optical signal transduction by responsive thin hydrogel films loaded with noble metal nanoparticles, *Advanced Materials*, **22**, pp. 1412..1416.
83. Endo, T., Ikeda, R., Yanagida, Y. and Hatsuzawa, T. (2008). Stimuli-responsive hydrogel-silver nanoparticles composite for development of localized surface plasmon resonance-based optical biosensor, *Analytica Chimica Acta*, **611**, pp. 205..211.
84. Bjork, P., Persson, N. K., Peter, K., Nilsson, R., Asberg, P. and Inganas, O. (2005). Dynamics of complex formation between biological and luminescent conjugated polyelectrolytes - a surface plasmon resonance study, *Biosensors & Bioelectronics*, **20**, pp. 1764..1771.
85. Nilsson, K. P. R. and Inganas, O. (2003). Chip and solution detection of DNA hybridization using a luminescent zwitterionic polythiophene derivative, *Nature Materials*, **2**, pp. 419..424.
86. Nilsson, K. P. R., Andersson, M. R. and Inganas, O. (2002). Conformational transitions of a free amino-acid-functionalized polythiophene induced by different buffer systems, *Journal of Physics: Condensed Matter*, **14**, pp. 10011..10020.
87. Yang, H. H., Liu, H. P., Kang, H. Z. and Tan, W. H. (2008). Engineering target-responsive hydrogels based on aptamer - target interactions, *Journal of the American Chemical Society*, **130**, pp. 6320..6321.
88. Zhu, Z., Wu, C. C., Liu, H. P., Zou, Y., Zhang, X. L., Kang, H. Z., Yang, C. J. and Tan, W. H. (2010). An aptamer cross-linked hydrogel as a colorimetric platform for visual detection, *Angewandte Chemie International Edition*, **49**, pp. 1052..1056.
89. Matsui, J., Takayose, M., Akamatsu, K., Nawafune, H., Tamaki, K. and Sugimoto, N. (2009). Molecularly imprinted nanocomposites for highly sensitive SPR detection of a non-aqueous atrazine sample, *Analyst*, **134**, pp. 80..86.